Remote Sensing of Environment 113 (2009) 1988–1999

Contents lists available at ScienceDirect

Remote Sensing of Environment

journal homepage: www.elsevier.com/locate/rse

Generation of dense time series synthetic Landsat data through data blending with MODIS using a spatial and temporal adaptive reflectance fusion model

Thomas Hilker [a,*], Michael A. Wulder [b], Nicholas C. Coops [a], Nicole Seitz [b], Joanne C. White [b], Feng Gao [c], Jeffrey G. Masek [c], Gordon Stenhouse [d]

[a] Department of Forest Resource Management, University of British Columbia, 2424 Main Mall, University of British Columbia, Vancouver, British Columbia, Canada V6T 1Z4
[b] Canadian Forest Service (Pacific Forestry Centre), Natural Resources Canada, Victoria, British Columbia, Canada V8Z 1M5
[c] Biospheric Sciences Branch, NASA Goddard Space Flight Center, Greenbelt MD, 20771, USA
[d] Foothills Research Institute, Hinton, Alberta, Canada T7V 1X6

ARTICLE INFO

Article history:
Received 29 August 2008
Received in revised form 20 May 2009
Accepted 22 May 2009

Keywords:
Landsat
MODIS
Synthetic imagery
STARFM
Data blending
EOSD

ABSTRACT

Landsat imagery with a 30 m spatial resolution is well suited for characterizing landscape-level forest structure and dynamics. While Landsat images have advantageous spatial and spectral characteristics for describing vegetation properties, the Landsat sensor's revisit rate, or the temporal resolution of the data, is 16 days. When considering that cloud cover may impact any given acquisition, this lengthy revisit rate often results in a dearth of imagery for a desired time interval (e.g., month, growing season, or year) especially for areas at higher latitudes with shorter growing seasons. In contrast, MODIS (MODerate-resolution Imaging Spectroradiometer) has a high temporal resolution, covering the Earth up to multiple times per day, and depending on the spectral characteristics of interest, MODIS data have spatial resolutions of 250 m, 500 m, and 1000 m. By combining Landsat and MODIS data, we are able to capitalize on the spatial detail of Landsat and the temporal regularity of MODIS acquisitions. In this research, we apply and demonstrate a data fusion approach (Spatial and Temporal Adaptive Reflectance Fusion Model, STARFM) at a mainly coniferous study area in central British Columbia, Canada. Reflectance data for selected MODIS channels, all of which were resampled to 500 m, and Landsat (at 30 m) were combined to produce 18 synthetic Landsat images encompassing the 2001 growing season (May to October). We compared, on a channel-by-channel basis, the surface reflectance values (stratified by broad land cover types) of four real Landsat images with the corresponding closest date of synthetic Landsat imagery, and found no significant difference between real (observed) and synthetic (predicted) reflectance values (mean difference in reflectance: mixed forest $\bar{x}=0.086$, $\sigma=0.088$, broadleaf $\bar{x}=0.019$, $\sigma=0.079$, coniferous $\bar{x}=0.039$, $\sigma=0.093$). Similarly, a pixel based analysis shows that predicted and observed reflectance values for the four Landsat dates were closely related (mean $r^2=0.76$ for the NIR band; $r^2=0.54$ for the red band; $p<0.01$). Investigating the trend in NDVI values in synthetic Landsat values over a growing season revealed that phenological patterns were well captured; however, when seasonal differences lead to a change in land cover (i.e., disturbance, snow cover), the algorithm used to generate the synthetic Landsat images was, as expected, less effective at predicting reflectance.

1. Introduction

Vegetation canopy biophysical and structural information are required inputs to many landscape-scale models, including ecosystem process and wildlife habitat models (Peddle et al., 1999; Sellers, 1985; Sellers et al., 1996; Townshend & Justice, 1995). Since the launch of the first satellite sensors in the 1970s, remote sensing has emerged as a key technology for providing modeling inputs in a spatially continuous fashion, with considerable progress being made in the determination of biophysical plant properties from optical sensors (Prince, 1991; Prince & Goward, 1995; Eklundh et al., 2001; Patenaude et al., 2005; Masek & Collatz, 2006). Key challenges are still imposed by technological limitations, requiring trade-offs to be made between the spatial, spectral, and temporal resolutions of an instrument, and often preventing an adequate description of ecosystem dynamics and disturbance for modeling purposes. For instance, high spatial resolution typically results in a smaller image footprint, or spatial extent, thereby increasing the time it takes a satellite to revisit the same location on Earth (Coops et al., 2006). Conversely, high temporal resolution sensors have a more frequent revisit rate and produce wide-area coverage with a lower spatial resolution (Holben, 1986; Justice et al., 1985).

* Corresponding author. Department of Forest Resource Management, Forest Sciences Centre. 2424 Main Mall University of British Columbia, Vancouver, British Columbia, Canada V6T 1Z4. Tel.: +1 604 822 4148; fax: +1 604 822 9106.
E-mail address: thilker@interchange.ubc.ca (T. Hilker).

0034-4257/$ – see front matter © 2009 Elsevier Inc. All rights reserved.
doi:10.1016/j.rse.2009.05.011

Arguably, the most commonly used satellite sensor for mapping biophysical vegetation parameters and land cover type is Landsat (Cohen & Goward, 2004). The Landsat TM and ETM+ sensors on board the Landsat 5 and 7 platform have a spatial resolution of 30 m, a spatial extent of 185×185 km per scene, and proven utility for monitoring land cover and land cover changes (Wulder et al., 2008). Its 16-day revisit-cycle, however, which can be significantly lengthened due to cloud contamination (Ju & Roy, 2007), can limit Landsat's use for monitoring biodynamics (Ranson et al., 2003; Roy et al., 2008) and may create difficulties in mapping vegetation conditions in a timely manner (Gao et al., 2006; Leckie, 1990; Pape & Franklin, 2008). The impact of clouds on satellite imagery can be of major concern (Ju & Roy, 2007), especially notably in tropical locations and regions with variable topography. For instance, Leckie (1990) found that the probability of acquiring a cloud-free Landsat scene (cloud cover <10%) can be as low as 10% for some regions in Canada (observed during July and August); plus, technical difficulties, such as the scan line corrector failure of the Landsat ETM+ sensor in 2003 (Maxwell et al., 2007), can further reduce the availability of images suitable for analysis.

Changes in land cover and ecosystem disturbance are important drivers of habitat distribution and species abundance (Pape & Franklin, 2008) and as a result, a goal for terrestrial monitoring, especially habitat mapping, is to have both high spatial and temporal resolutions. One possible way to meet this goal is through fusing data from sensors with differing spatial and temporal characteristics. In general, data fusion or data blending combines multi-source satellite data to generate information with high spatial and temporal resolution. Several approaches describing existing fusion techniques are summarized in Table 1. An early example of a fusion model was illustrated by Carper et al. (1990) who combined 10 m spatial resolution SPOT panchromatic imagery with 20 m spatial resolution multispectral imagery by using an intensity–hue-saturation (IHS) transformation. The generated composite images have the spatial resolution of the panchromatic data and the spectral resolution of the original multispectral data. Other techniques to enhance the spatial resolution of multispectral bands include component substitution (Shettigara, 1992), and wavelet decomposition (Yocky, 1996). One of the first studies designed to increase the spatial resolution of MODIS using Landsat was introduced by Acerbi-Junior et al. (2006) using wavelet transformations. The algorithm yields classified land cover types and was used for mapping the Brazilian Savanna (Acerbi-Junior et al., 2006). Recently, Hansen et al. (2008) used regression trees to fuse Landsat and MODIS data based on the 500 m 16-day MODIS BRDF/Albedo land surface characterization product (Roy et al., 2008; Hansen et al., 2008) to monitor forest cover in the Congo Basin on a 16-day basis.

Table 1
Summary of data blending techniques found in the literature.

Technique	Sensor 1	Scale 1 (m)	Sensor 2	Scale 2 (m)	Author
IHS Transforms	SPOT Pan	10	Spot XS	20	Carper et al., (1990)
Component Substitution	XS SPOT	20	SPOT Pan	10	Shettigara (1992)
	Landsat TM	30	SPOT Pan	10	
Multi-resolution wavelet decomposition	Landsat TM	28.5–120	SPOT Pan	10	Yocky (1996)
Wavelet Transforms	MODIS 1,2	250	Landsat TM	30	Acerbi-Junior et al., (2006)
	MODIS 3–7	500			
Downscaling MODIS	MODIS 1,2	250	MODIS 3–7	500	Trishchenko et al. (2006)
Combining medium and coarse-resolution satellite data	MODIS	250	Landsat TM	30	Busetto et al. (2007)
Semi-physical data fusion approach using MODIS BRDF/Albedo	MODIS	500	Landsat TM	30	Roy et al., 2008; Hansen et al., 2008
STARFM	MODIS	500	Landsat TM	30	Gao et al. (2006)

Pan = Panchromatic, XS = Multi-spectral.

Table 2
Comparison of spectral bands of Landsat TM/ETM+ and MODIS sensors.

Landsat		Band name	MODIS	
Band	Spectral range		Band	Spectral range
1	450–520 nm	Blue	3	459–479 nm
2	520–600 nm	Green	4	545–565 nm
3	630–690 nm	Red	1	620–670 nm
4	760–900 nm	Near IR	2	841–876 nm
5	1550–1750 nm	Mid IR	6	1628–1652 nm
7	2080–2350 nm	Mid IR	7	2105–2155 nm

While there are numerous examples existing in the current literature that fuse data from multiple sensors, only a few techniques yield calibrated outputs of spectral radiance or reflectance (Gao et al., 2006), a requirement to study vegetation dynamics or quantitative changes in reflectance over time. The Spatial and Temporal Adaptive Reflectance Fusion Model (STARFM) (Gao et al., 2006) is one such model and was designed to study vegetation dynamics at a 30 m spatial resolution. STARFM predicts changes in reflectance at Landsat's spatial and spectral resolution using high temporal frequency observations from MODIS. STARFM predicts reflectance at up to daily time steps, depending on the availability of MODIS data. MODIS sensors are present on the polar orbiting Terra and Aqua spacecrafts, launched in 1999 and 2002 respectively, and acquire data in 36 spectral bands, 7 of which are commonly used for terrestrial applications (Wolfe et al., 2002). Depending on the spectral channel of interest, MODIS has spatial resolutions of 250 m, 500 m, and 1 km at nadir, with near daily global coverage.

STARFM was initially tested to predict daily Landsat-scale reflectance in the red and NIR region using the 500-m daily surface reflectance product (MOD09GHK) with one or more pairs of Landsat and MODIS images acquired on the same date (T_1) and one or more MODIS observations from the prediction date (T_2) (Gao et al., 2006). For more humid areas of the Earth, which are frequently cloud contaminated, it can, however, be useful to base the predictions on multi-day composites, such as provided by the 8-day MOD09A1/MYD09A1 product, to minimize cloud contamination in existing MODIS scenes (Vermote & Kotchenova, 2008). Spectral information from the Landsat ETM+ sensor is synthesized by matching the locations of Landsat ETM+ bands 1–5 and 7 to their corresponding MODIS land bands (Table 2) (Gao et al., 2006).

In the study presented herein, we build upon the work of Gao et al. (2006) and investigate the suitability of the STARFM algorithm for generating synthetic Landsat images that may then be used to investigate vegetation dynamics in different land cover types. We assess the quality of the synthetic (predicted) Landsat reflectance values for a number of broad vegetation classes (mainly coniferous forest), by comparing these predictions with reflectance values from real (observed) Landsat images acquired throughout one growing season. The objective of this study is to investigate the potential of STARFM for assessing seasonal changes (i.e. changes due to vegetation green-up and leaf senescence) in vegetation cover and vegetation status in the boreal and sub-boreal forest regions for which the potential of acquiring frequent higher spatial resolution data (and therefore the potential for mapping of vegetation dynamics) is otherwise low. Algorithms like the one used in this study are important components of current research efforts seeking to map high spatial resolution changes in vegetation cover and status with high temporal density, over larger areas. Data blending approaches, such as STARFM can help in minimizing the technical limitations and trade-offs associated with information needs that require data with both high spatial and high temporal resolutions. Applications such as monitoring seasonal changes in vegetation biophysical and structural attributes over large areas can benefit from the synergies of multiple data sources such as MODIS and

Landsat. Advances in data blending can also influence the design of new sensors, where the advantages of different spatial and temporal resolutions may be fully realized in the creation of different sensors on different platforms, with the complementary nature of these systems in a data blending approach, considered from the outset of the design process.

2. Methods

2.1. Study area and image data

Criteria for site selection included the availability of four or more consecutive Landsat images in the growing season of a given year with less than 10% cloud cover. Our study area is the Landsat WRS-2 Path 47/Row 24, centered at approximately 51° 41′ 00′ N latitude and 121° 37′ 00″ W longitude, located in central British Columbia, Canada (Fig. 1). The 185 × 185 km study area intersects with the 100 Mile House and Central Cariboo Forest Districts of the Southern Interior Forest Region. The vegetation in this area is dominated by coniferous tree species, including Douglas-fir (*Pseudotsuga menziesii*, Mirbel), lodgepole pine (*Pinus contorta* var. *latifolia,* Douglas ex Loudon) and white spruce (*Picea glauca*, (Moench) Voss). The climate in this area is extreme, with characteristically hot, moist summers and cold winters, which often have large amounts of snow accumulation (Meidinger & Pojar, 1991).

Five cloud-free Landsat scenes acquired between May and mid October 2001 were available for the study site and were acquired through the USGS GLOVIS portal (http://glovis.usgs.gov/). Images were atmospherically corrected using the cosine approximation model (COST) (Wu et al., 2005) and radiometrically normalized (Hall et al., 1991) with respect to the 2005 imagery in order to simplify the comparison between the data. The registration accuracies (RMS error) for the five Landsat scenes were 0.47 m for the image acquired on May 6, 2001 and 0.49 m for the images acquired on July 9, Aug 10 and Sept 27, 2001.

Additionally, 19 eight-day MODIS composites (MOD09A1, using data from the Terra platform) for the same time period and with a spatial resolution of 500 m were obtained from the EOS data gateway of NASA's Goddard Space Flight Center (http://redhook.gsfc.nasa.gov). Fig. 2 contains an overview of the Landsat and MODIS scenes used in this study. Following STARFM algorithm input requirements, the MODIS data were reprojected to the Universal Transverse

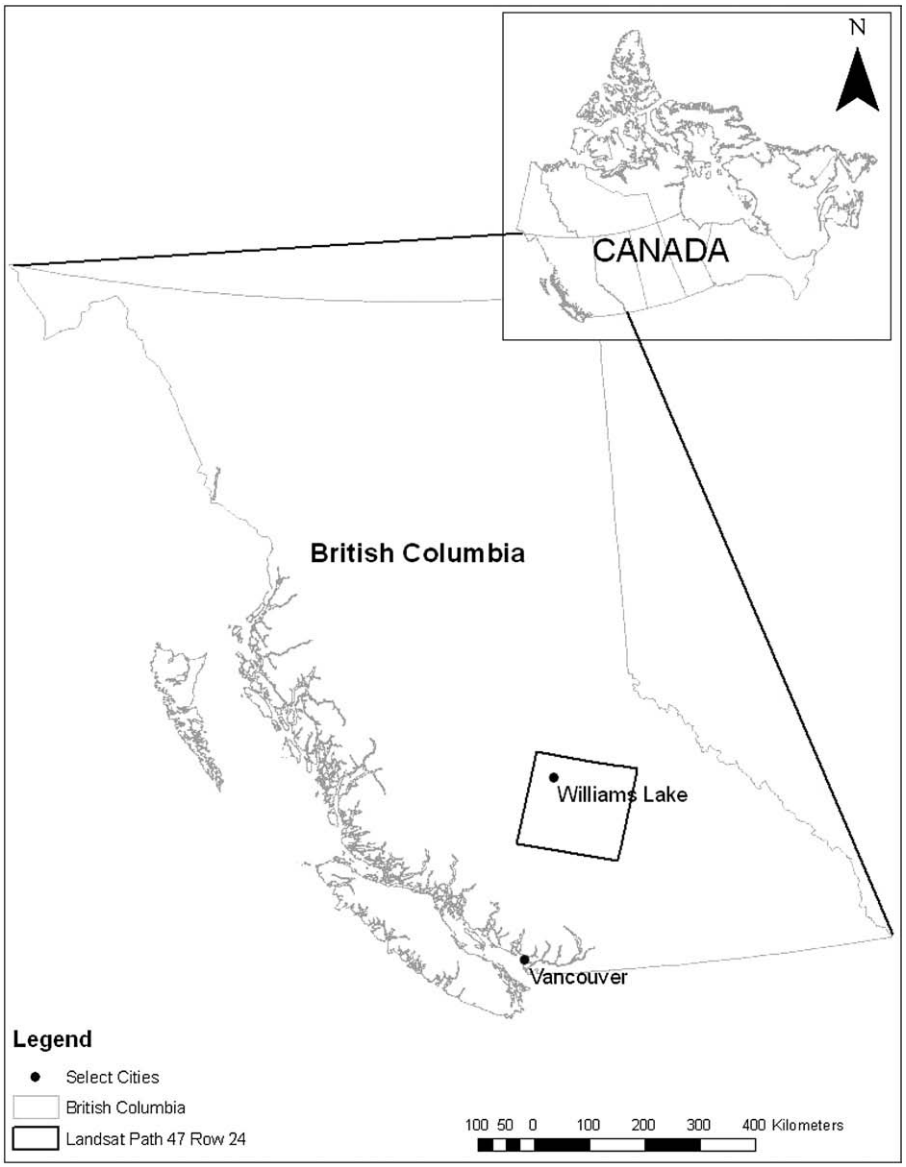

Fig. 1. Map of the study area. The study site encompasses a Landsat scene (185 × 185 km^2 near Williams Lake BC, Canada.

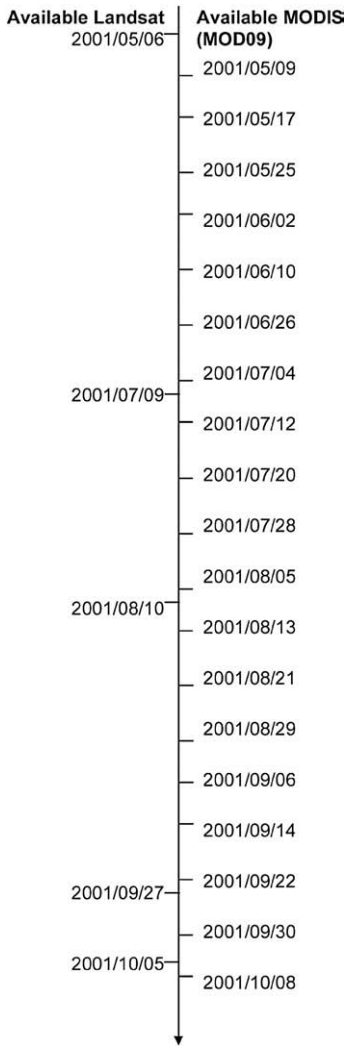

Fig. 2. Acquisition dates of Landsat and MODIS scenes used for this study. Note that MODIS data were acquired as 8-day composites, the dates given in the figure are the first day of the 8-day acquisition period, respectively.

Mercator (UTM) projection using the MODIS reprojection tool (Kalvelage & Willems, 2005), clipped to the extent of the available Landsat imagery, and resampled to a 30 m spatial resolution using a nearest neighbour approach.

2.2. Land cover classification

A Landsat derived land cover classification product developed by the Earth Observation for Sustainable Development of Forests (EOSD) initiative, a joint collaborative between the Canadian Forest Service and the Canadian Space Agency, provided information on land cover types in the study area (Wulder et al., 2003). The EOSD product is based upon the unsupervised classification, hyperclustering, and manual labelling of Landsat data, facilitating the classification of land cover types over larger areas (Franklin & Wulder, 2002; Slaymaker et al., 1996; Wulder et al., 2003). The EOSD product represents 23 unique land cover classes mapped at a spatial resolution of 0.0625 ha (equivalent to a 25 m by 25 m pixel) thereby representing circa year 2000 conditions (Wulder et al., 2008). The accuracy of the EOSD product was found to be 77%, achieving a target accuracy of 80%, with a 90% confidence interval of 74–80% (for more detailed information see Wulder et al., 2007).

EOSD land cover data for the study area were downloaded from the EOSD data portal (http://www4.saforah.org/eosdlcp/nts_prov.html) and resampled to a 30 m resolution using a nearest neighbour approach. The dominant land cover type in the study area is coniferous forest (comprised of Douglas-fir, lodgepole pine, and white spruce) with subsidiary herbal and shrub vegetation and patches of water and rocks. Land cover patches are generally large, the landscape can, however, be quite heterogeneous within some areas due to harvesting activities and related cut-blocks and access road networks. About 1.8% of the study area has not been classified due to cloud contamination during acquisition of the Landsat scene used for EOSD classification. This area has been excluded from data analysis. The classification accuracy for coniferous and deciduous forests and their associated density classes is ~92%, the mixed forest class is classified with ~88% accuracy (Wulder et al., 2003).

2.3. Data processing using STARFM

STARFM predicts pixel values based upon a spatially weighted difference computed between the Landsat and the MODIS scenes acquired at T_1, and the Landsat T_1-scene and one or more MODIS scenes of prediction day (T_2), respectively (Gao et al., 2006). A moving window technique is used to minimize the effect of pixel outliers thereby predicting changes of the center pixel using the spatially and spectrally weighted mean difference of pixels within the window area (Gao et al., 2006). The prediction algorithm in STARFM is given by (Gao et al., 2006),

$$L\left(x_{w/2}, y_{w/2}, T_2\right) = \sum_{i=1}^{w}\sum_{j=1}^{w} W_{ij}\left(M\left(x_i, y_j T_2\right) + L\left(x_i, y_j T_1\right) - M\left(x_i, y_j T_1\right)\right) \quad (1)$$

where $L(x_{w/2}, y_{w/2}, T_2)$ is a Landsat pixel value predicted for the time T_2, w is the size of the moving window and $x_{w/2}$, $y_{w/2}$ is the central pixel within this moving window. The spatial weighting function W_{ij} determines how much each neighbouring pixel (x_i,y_j) in w contributes to the estimated reflectance of the central pixel. $M(x_i, y_jT_2)$ is the MODIS reflectance at the window location (x_i, y_j) observed at T_2, while $L(x_i, y_jT_1)$ and $M(x_i, y_jT_1)$ are the corresponding Landsat and MODIS reflectance values observed at the base date T_1, respectively (Gao et al., 2006). The weighting function implemented in STARFM (when based on a single Landsat and MODIS image as T_1 input) is calculated from the product (C_{ij}) of the spectral ($S_{i,j}$) and spatial distance ($D_{i,j}$) between the central predicted pixel and the surrounding candidate pixel. W_{ij} is calculated as the normalized reverse function of this product (Gao et al., 2006).

$$W_{i,j} = \left(1 / C_{ij} / \sum_{i=1}^{w}\sum_{j=1}^{w}\left(1 / C_{ij}\right)\right) \quad (2)$$

An area of 1500 m × 1500 m was selected as the moving window size for STARFM predictions (Gao et al., 2006). The uncertainties of Landsat and MODIS surface reflectance were set to 0.002 and 0.005 for the visible and the NIR bands, respectively (Gao et al., 2006). Synthetic Landsat images were predicted using the Landsat scene acquired at 2001/08/10 in conjunction with the MODIS scene acquired at 2001/08/13 as T_1 data. T_2 was defined as the dates for which the remaining 18 MODIS 8-day composites were available. The August MODIS and Landsat image pair was selected as T_1 input because it had the least amount of cloud cover (close to 0%), and because the temporal difference between the MODIS and the corresponding Landsat scene was minimal (reducing the likelihood for changes in land cover resulting from harvesting or phenological changes).

Clouds in Landsat data were flagged by means of a cloud mask algorithm (Irish, 2000; Irish et al., 2006), which uses subsequent filtering techniques to identify cloud contamination in Landsat data based on pixel brightness, surface temperature and several band ratios

to eliminate highly reflective vegetation, senescing vegetation, and highly reflective rocks and sands (Irish, 2000; Irish et al., 2006). Clouds in the MODIS imagery were identified using the MODIS quality flags. Low quality pixels (such as snow or cloud contaminated) in either Landsat or MODIS data were predicted in STARFM but excluded from the statistical analysis.

2.4. Assessment of STARFM synthetic Landsat imagery

The four remaining Landsat scenes were used for validation (cross-comparison) to allow assessment of the quality of the STARFM predictions (real to synthetic Landsat images) made throughout the 2001 growing season. The prediction accuracy was assessed on a per-pixel basis by comparing the reflectances of observed and predicted Landsat images for a subset of the study area (random sample of 10% of the vegetated land surface area). The prediction quality of STARFM was assessed from the difference between observed and predicted scenes by comparing the 4 image pairs on a pixel by pixel basis and per land cover type defined from the EOSD land cover product. A two-sided *t*-test of the difference images was used to determine whether there is a statistically significant difference between observed and predicted reflectance values (i.e., whether the mean difference between observed and predicted data varied significantly from zero).

Changes in vegetation green-up and leaf-down were described using the normalized difference vegetation index (NDVI) (Tucker, 1979), as one of the most commonly used measures of vegetation cover and leaf area (Asrar et al., 1984; Daughtry et al., 1983; Myneni & Williams, 1994; Sellers 1985). NDVI was calculated per land cover class for all 18 prediction dates and then compared to the Landsat observed NDVI values at the 4 validation dates throughout the 2001 growing season.

3. Results

Table 3 shows the percent coverage of the different land cover types found within the study area. The majority of land is covered by open and sparse coniferous forest, while mixed and broadleaf forest types only cover about 4% of the study area. The STARFM algorithm yielded 18 high spatial resolution, synthetic Landsat images for the 2001 growing season (May through October) using a Landsat and a MODIS scene acquired in August 2001 as the T_1 images, and 18 eight-day MODIS composites between May and October 2001 as the T_2 images for prediction. Fig. 3 shows the five observed Landsat scenes (4A, 4D, 4G, 4J, 4M), the corresponding MODIS composites used for STARFM predictions (4B, 4E, 4H, 4K, 4N), and the predicted synthetic Landsat images in the right column (4C, 4F, 4L, 4O). No image was synthesized for August 13, as the August imagery was used as T_1 input. Larger, visible differences in Fig. 3 were due to cloud contamination in the Landsat and MODIS scenes and, in the case of the May image, snow cover. The quality of the synthetic Landsat images was affected by cloud contamination in the T_2 MODIS composites, resulting in a few streaking effects in the synthesized images, particularly in the shorter wavebands (Fig. 3C and O, upper portion of the image). Fig. 4 shows an example of a 10×10 km subset of the Landsat scene obtained in July (Fig. 4A) and the corresponding STARFM synthetic image (Fig. 4B). STARFM maintained a high level of spatial detail in the predicted scenes, including areas with more heterogeneous and complex land cover types. The spatial patterns related to differing land cover types were well maintained in the synthetic images (Fig. 4). Fig. 5A–L shows a per-pixel comparison between observed and predicted Landsat reflectance for the focus area shown in Fig. 4. The rows represent the reflectance values for the NIR, red and green TM band, respectively, the columns represent the four validation dates (May 9, July 12, September 30 and October 08). Highest correlations between observed and predicted pixel values were found for the NIR band ($0.73<r^2<0.82$; $p<0.01$) (Fig. 5A–D), while the shorter wavebands in the visible part of the spectrum yielded weaker relationships. The coefficients of determination ranged between $0.27<r^2<0.67$ for the red and between $0.44<r^2<0.62$ for the green band. Prediction accuracy was highest for the scenes predicted for July 12 and September 30 (Fig. 5B–C, F–G and J–K), while the precision was lower especially for the visible bands at the beginning of the vegetation period (Fig. 5E,I). The relationship between observed and predicted pixel values closely followed the 1-to-1 line (Fig. 5A–L) thereby showing that Landsat reflectance was accurately predicted by STARFM. Some deviations from this 1-to-1 line, however, were found for the red band towards the end of the vegetation period (Fig. 5H). Table 4 shows a pixel based comparison between observed and predicted Landsat images for TM bands 2–5 and NDVI summarized for the most important land cover categories, 1) shrub and herb, 2) forested vegetation and 3) all land cover types combined. The first column in each sub-table shows the coefficient of determination for the pixel based regression between the observed Landsat scenes (May 06, July 09, Sept 27 and Oct 05) and the STARFM predicted images whose prediction date was closest to the observed scenes (May 09, July 12, Sept 30 and Oct 08, respectively). The relationship between observed and predicted was highest for the longer wavebands (Red, NIR and SWIR, NDVI), and for the more heterogeneous land cover types, showing a larger range of pixel values. The second column shows the intercept of the relationship, data were normalized to the maximum observed reflectance of each band in order to facilitate a comparison between different wavelengths. STARFM consistently overestimated the intercept between 0 and 19% of the observed reflectance, best results were found for the longer wavelengths. The slope between observed and predicted pixel values followed the 1:1 line relatively close but the predicted values slightly underestimated the observed reflectance in all cases. Best results were found for NDVI band, likely due to the normalization of the indexed values.

Fig. 6A–D shows a quantitative comparison between the four real Landsat scenes used for validation (4A, 4D, 4J, 4M) and the corresponding synthesized scenes (4C, 4F, 4L, 4O), using ETM+ band 5 ($\rho=1550$–1750 nm) as an example. The mean deviation between the observed and predicted images ranged between 1.86 (July) and 4.06% of the observed image (September) with a standard deviation of 2.51 and 6.46% of the observed image, respectively. Statistical analysis (two-sided *t*-test,: $\alpha=0.05$, $p<0.0001$, sample size 1000 of randomly selected pixels, $t_{April}=1.5568$, $t_{July}=1.6566$, $t_{September}=1.5871$, $t_{October}=1.2578$ for ETM+ Band 3, $t_{April}=0.1242$, $t_{July}=-0.0905$, $t_{September}=0.5776$, $t_{October}=0.0086$ for ETM+ Band 4) showed that there is no statistically significant difference between the mean observed and predicted Landsat reflectance, for any of the EOSD cover types considered, when excluding areas with cloud and snow cover. The observed effect size (Cohen's *d*) was $<=0.4489$ which resulted in a type II error rate of 0.000.The colors correspond to the magnitude of the differences between observed and predicted

Table 3
EOSD-Land cover types and percent coverage found within the study area (185×185 km^2).

Land cover type	% cover
Shadow	1.01
Water	3.22
Snow/ice	0.28
Rock/rubble	0.22
Exposed land	4.49
Bryoids	0.00
Shrub tall	0.24
Shrub low	6.94
Wetland	1.84
Herb	9.31
Coniferous	66.79
Broadleaf	2.25
Mixed forest	1.58

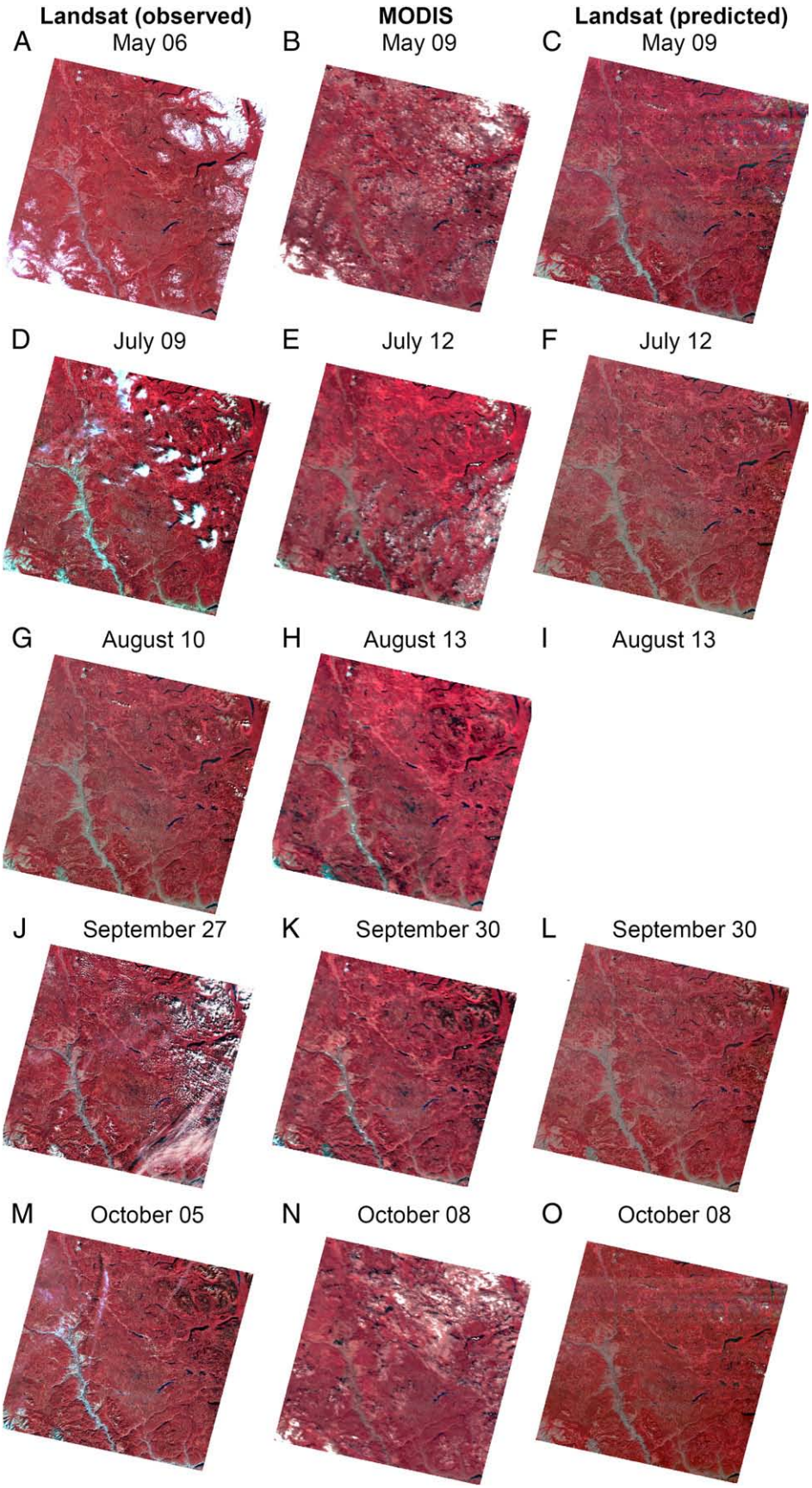

Fig. 3. Comparison between observed Landsat scene (left column), observed MODIS scene (central column) and predicted Landsat scene (right column) for the 5 acquisition dates. No synthetic data has been predicted for August 13 as the Landsat input data from August have been used as T_1 image (band combination: NIR, red, green.

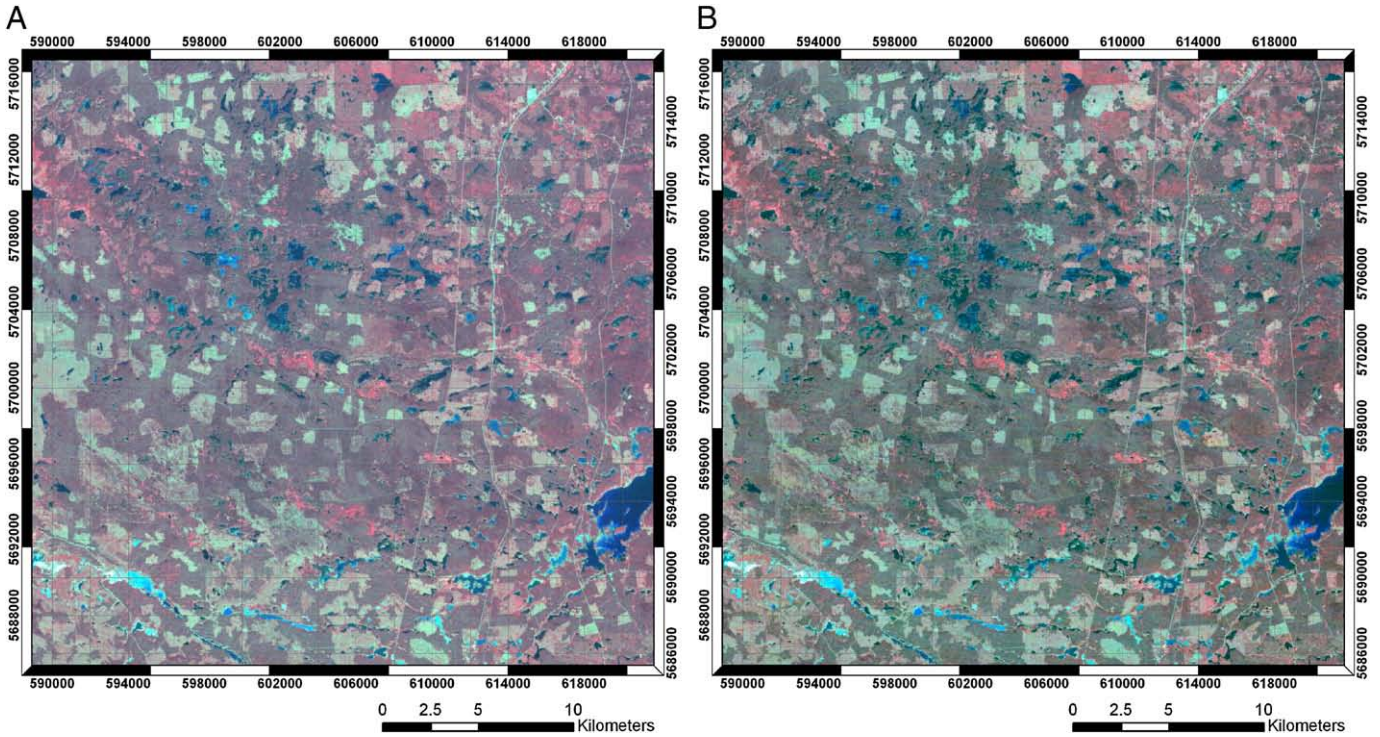

Fig. 4. Comparison of fine scale structure between observed Landsat scene (acquired July 09 2008) and predicted Landsat scene (predicted using July 12 as prediction date). STARFM was able to represent the heterogeneity of Landscape well.

images. Note that the major differences occurring in the images correspond to the cloud contamination present in the Landsat scenes (compare Figs. 3D (July 9) and 4J (Sept 27)).

Fig. 7A–F demonstrates the ability of STARFM to predict seasonal changes in vegetation reflectance. Data include only those pixels whose location coincides with vegetated land cover classes as defined by the EOSD map. Fig. 7A–C shows a comparison between the Landsat reflectance observed at May 6 and the Landsat reflectance observed at August 10, for the green (Fig. 7A), red (Fig. 7B) and NIR (Fig. 7C) bands, respectively. Seasonal changes in the reflectance in vegetation are visible in the red and NIR band, as the Landsat image observed in August underestimated the reflectance in the red and NIR part of the spectrum. Fig. 7D–F shows a comparison between the Landsat reflectance observed at May 6 and the reflectance values predicted for May 9 using STARFM (Figs. 7D–F represent the green, red and NIR band, respectively, again only those pixels whose location coincides with vegetated land cover types were included). The diagrams shown in Fig. 7D–F show a better fit to the 1-to-1 line than Fig. 7A–C as the additional information acquired from MODIS data helps to account for seasonal changes in reflectance of vegetation (Gao et al., 2006).

Fig. 8A–D shows a time series of the normalized difference vegetation index (NDVI) (Tucker, 1979) for the most common vegetation types found within the study area, derived from the synthetic Landsat images predicted using STARFM (sparse, open, and dense forest types are summarized into one class). NDVI values obtained from the real Landsat scenes are shown as open squares. Seasonal changes in vegetation status were well described by STARFM for all vegetation cover types, with best results found for the broadleaf vegetation class. For example, changes in physiological status of the canopy during the green-up period were well described by the algorithm and only small deviations were found between observed NDVI and STARFM predicted NDVI values throughout the growing season, with deviations from expectation evident for the MODIS image acquired outside the growing season in October (2001/10/08). As expected, greatest differences in seasonality were found for the broadleaf vegetation class ($\Delta NDVI_{max} = 0.21$), while the coniferous land cover type maintained a more homogeneous level of NDVI values throughout the observation period ($\Delta NDVI_{max} = 0.16$). The variability in mean and standard deviations of NDVI values of adjacent 8-day intervals was low, which suggest a high level of precision for the predicted NDVI values. The T_1 date in Fig. 8 is highlighted in grey as this date was used to illustrate the seasonal variation in STARFM predictions which was derived from the T_2 MODIS scene.

4. Discussion

This study investigated the capability of STARFM (Gao et al., 2006) to predict seasonal changes in different land cover types observed over a 34,225 km^2 study area in south-central British Columbia, Canada. STARFM was successfully used to predict 8-day synthetic Landsat images between May and October 2001 based on one Landsat and 18 MODIS observations (Fig. 3). The use of MODIS composite images rather than daily MODIS reflectance products yielded largely cloud-free predictions throughout the 2001 study period and can therefore help to predict changes in reflectance of vegetation in more humid areas of the Earth where cloud cover prevents frequent cloud-free observations. The use of MODIS composites rather than single observations may, however, impact the average reflectance brightness for a given image region, depending on the MODIS scenes used in the MOD09A1/MYD09A1 product and is therefore at the same time also a limitation to the applied technique as the composition of data originating from multiple viewing angles and the variation of vegetation within the 8-day production period which differs from the Landsat acquisition date, also provides a possible source of error.

STARFM maintained a high level of spatial detail in the predicted scenes (Fig. 4). The algorithm was particularly effective at predicting the reflectance values for the vegetated land cover types, with differences between observed and predicted values being less than 4% of the observed reflectance (Fig. 6). The high level of spatial detail maintained by the STARFM predictions (Fig. 4) is indicative of the

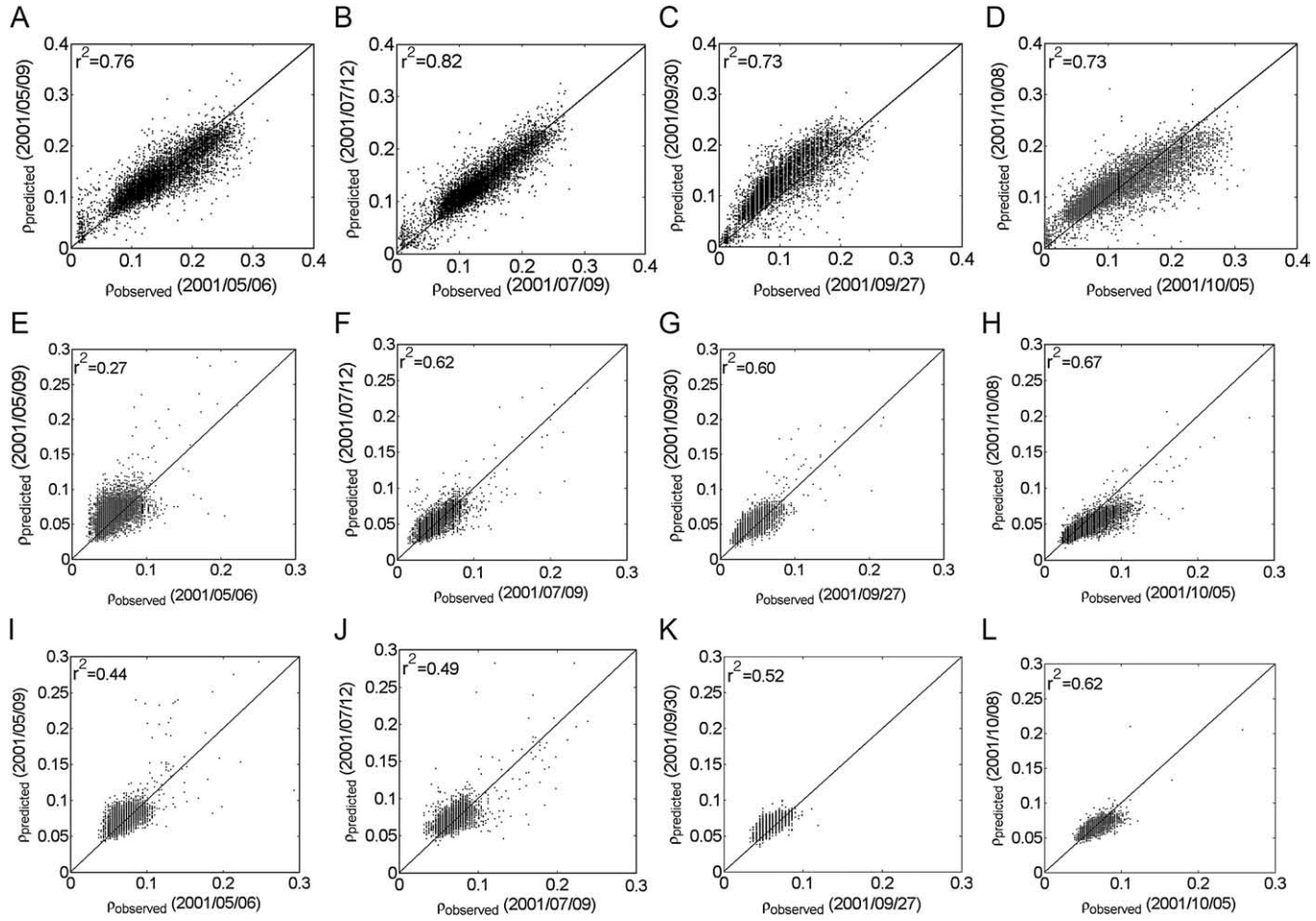

Fig. 5. Per-pixel comparison between observed and predicted Landsat reflectance. The rows represent the reflectance values for the NIR, red and green TM band, respectively, the columns represent the four validation dates. Highest correlations between observed and predicted pixel values were found for the NIR band ($0.73<r^2<0.82$; $p<0.01$) (A–D), while the visible reflectances yielded weaker relationships ($0.27<r^2<0.67$ for the red (E–H), and $0.44<r^2<0.62$ for the green band (I–L)) ($p<0.01$). Prediction accuracy was highest for the scenes predicted for July 12 and September 30 (B–C, F–G and J–K), while the accuracy was lower especially for the visible bands at the beginning of the vegetation period (E and I).

quality of the predicted scenes with spatial changes in landscape patterns well maintained by the algorithm, even in areas with more heterogeneous, complex land cover types.

Highly significant correlations were found between observed and predicted pixel values for all the examined wavebands and land cover types (Fig. 5, Table 4). These findings are also confirmed by previous

Table 4
Pixel based regression of the observed Landsat scenes (May 06, July 09, Sept 27 and Oct 05) versus the STARFM predicted images that whose prediction date was closest to the observed scenes (May 09, July 12, Sept 30 and Oct 08).

	TM band	May 06			July 09			Sept 27			Oct 05		
Land cover	2	r^2	a	b	r^2	a	b	r^2	a	b	r^2	a	b
Herb/shrub		0.55	0.03	0.93	0.67	0.09	0.82	0.66	0.07	0.84	0.69	0.12	0.78
Forest		0.42	0.14	0.69	0.57	0.13	0.77	0.59	0.12	0.78	0.64	0.10	0.78
Combined		0.47	0.09	0.77	0.60	0.11	0.76	0.61	0.10	0.80	0.65	0.12	0.77
Land cover	3	r^2	a	b	r^2	a	b	r^2	a	b	r^2	a	b
Herb/shrub		0.61	0.05	0.90	0.70	0.09	0.83	0.68	0.09	0.84	0.64	0.12	0.78
Forest		0.53	0.12	0.74	0.63	0.11	0.79	0.69	0.10	0.83	0.73	0.09	0.84
Combined		0.56	0.09	0.80	0.66	0.10	0.80	0.69	0.08	0.83	0.69	0.09	0.82
Land cover	4	r^2	a	b	r^2	a	b	r^2	a	b	r^2	a	b
Herb/shrub		0.79	0.04	0.90	0.85	0.04	0.92	0.75	0.07	0.87	0.73	0.07	0.85
Forest		0.47	0.16	0.70	0.59	0.12	0.78	0.51	0.14	0.79	0.51	0.16	0.78
Combined		0.71	0.07	0.85	0.78	0.06	0.88	0.67	0.08	0.81	0.67	0.10	0.80
Land cover	5	r^2	a	b	r^2	a	b	r^2	a	b	r^2	a	b
Herb/shrub		0.82	0.03	0.90	0.85	0.05	0.92	0.73	0.07	0.86	0.53	0.19	0.73
Forest		0.76	0.07	0.86	0.80	0.05	0.89	0.70	0.08	0.82	0.62	0.13	0.75
Combined		0.81	0.05	0.90	0.83	0.05	0.90	0.70	0.07	0.84	0.61	0.14	0.71
Land cover	NDVI	r^2	a	b	r^2	a	b	r^2	a	b	r^2	a	b
Herb/shrub		0.84	0.04	0.88	0.93	0.04	0.92	0.91	0.06	0.86	0.85	0.08	0.82
Forest		0.50	0.08	0.86	0.84	0.14	0.92	0.64	0.13	0.74	0.82	0.15	0.86
Combined		0.67	0.10	0.80	0.83	0.04	0.91	0.80	0.06	0.87	0.80	0.05	0.90

The first column in each sub-table is showing the coefficient of determination, the second column is showing the intercept, normalized to percent total reflectance of the observed image (for instance a value of 0.1 means the predicted image overestimated the reflectance by 10%), the third column is showing the slope of the relationship between observed and predicted.

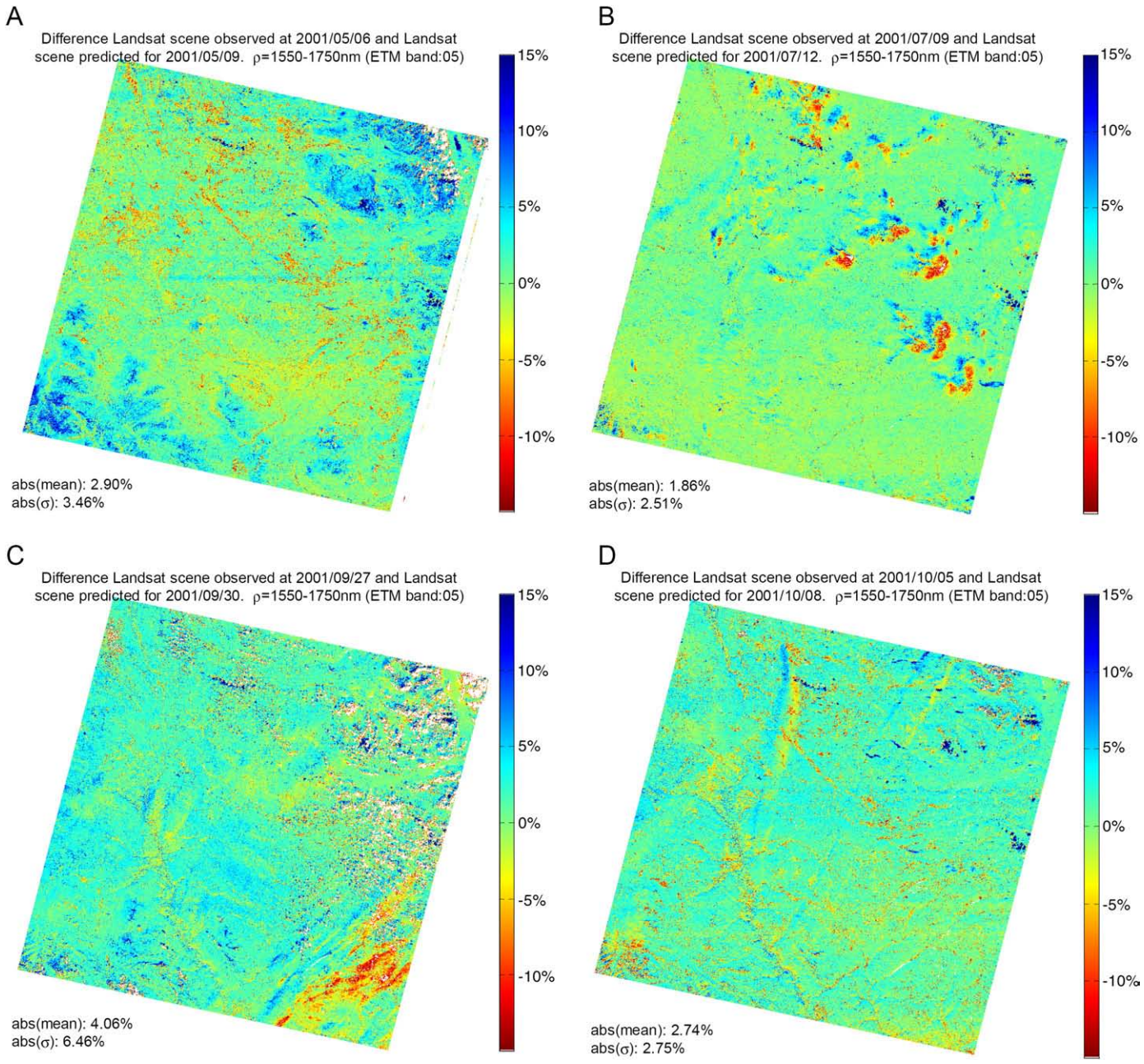

Fig. 6. Difference image between synthetic Landsat scenes predicted for 2001/05/09, 2001/07/09, 2001/09/27 and 2001/10/05 and corresponding Landsat scene. The difference between Landsat scene predicted for 2001/08/10 and observed at 2001/08/05 is not shown as $T_1 = T_2$. Red areas show cloud cover existing in the T_2 Landsat scene but not in the T_1 images, whereas blue areas show cloud cover in the T_1 scene but not in the T_2 scene. For areas clouded at either T_1 or the T_2, no reliable prediction can be made, hence clouded areas were excluded from any image statistics.

studies (Gao et al., 2006). Predictions of shorter wavebands, however, were found to be less precise than those made for the NIR region. This likely reflects the greater impact of atmospheric contamination at shorter wavelengths which has been reported to affect the prediction accuracy also for other fusion techniques (Roy et al., 2008). Atmospheric effects may also have impacted the significance of the relationship between observed and predicted reflectance as shown in Table 4 as the most significant relationships were found for the longer wavebands. In all cases the intercept of the relationship between observed and predicted images was >0 (Table 4, Fig. 5) which can be interpreted as a noise signal likely due to atmospheric and BRDF effects. The range of values is larger in the NIR region than for the visible bands (Fig. 5A–D, E–L), thus making the residuals of the NIR predictions relatively smaller (Table 4). As a result, land cover types with a greater range in pixel values (shrub, herb and all classes combined) showed a higher correlation between observed and predicted reflectance than the forested land cover class with relatively homogenous reflectance dominated by green tree crowns (Table 4).

The slopes of the relationship shown in Figs. 5A–L and 8D–F and Table 4 were consistent and slightly smaller than one for all prediction dates, thereby suggesting that seasonal effects have been accurately predicted using STARFM (Gao et al., 2006). The comparison between Figs. 7A–C and 8D–F demonstrates the gain of information by using MODIS data to account for seasonal changes in the reflectance of the vegetated land surface. These findings are confirmed also in Fig. 8 and demonstrate that STARFM was able to synthesize data that capture the seasonal variation in vegetation reflectance and the associated changes in biophysical and structural vegetation conditions. Vegetation green-up and leaf-down at the beginning and at the end of the vegetation period were well described by the synthesized NDVI

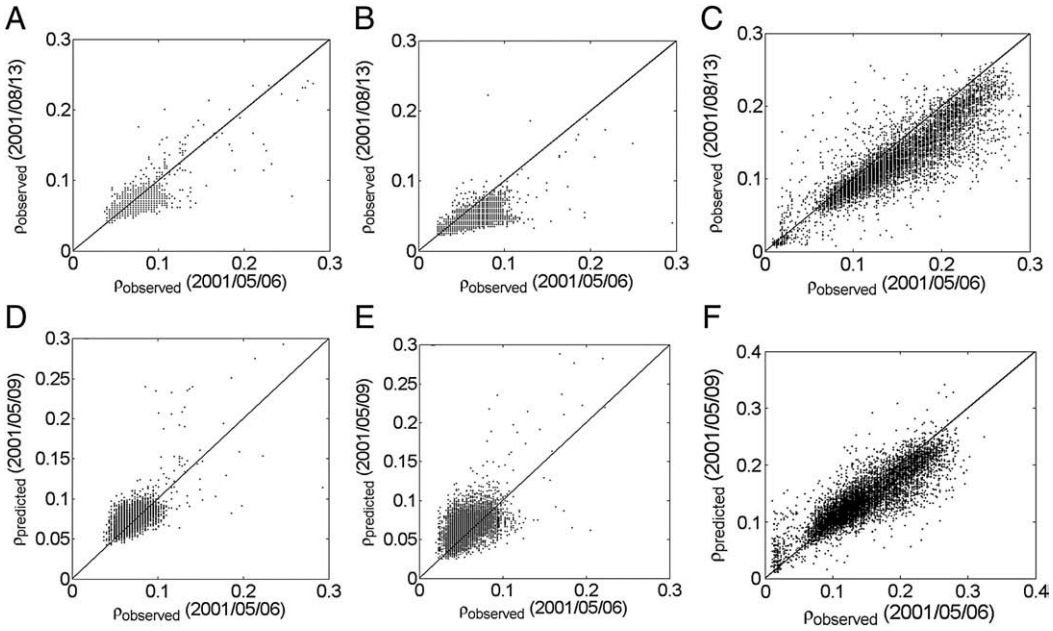

Fig. 7. A–F: Capability of STARFM to predict seasonal changes in reflectance. Data include only those pixel values whose location coincided with vegetated land cover classes as defined by the EOSD maps. A–C: Comparison between the Landsat TM reflectance observed at May 6 and the Landsat TM reflectance observed at August 10, for the green (A), red (B) and NIR (C) band. D–F: Comparison between the Landsat TM reflectance observed at May 6 for the green (D), red (E) and NIR (F) bands. The diagrams shown in D–F show a better fit to the 1-to-1 line than those in A–C.

values. The similarity to the NDVI computed from the observed images (Fig. 8, open squares) shows that the synthetic data are useful to quantify seasonal changes in reflectance induced by physiological changes in vegetation (Drake, 1976; Tucker, 1979; Sellers, 1985) at fine spatial scales (Gao et al., 2006).

The predictability of changes in the fine resolution synthetic images depends upon the capacity of MODIS to detect these changes, particularly when they occur in vegetation structure or stand composition or at sub-pixel ranges (Gao et al., 2006). For instance, pixel brightness of fine resolution predictions can only be adjusted at coarse-resolution scales. Consequently, it will be difficult to identify or spatially define individual change events as it is not possible to depict changes occurring in the sub-MODIS pixel range. As a result, the algorithm in its current form seems less suited (and was not designed) for the prediction of changes in vegetation structure (such as originating from clear cut harvesting or thinning) or changes in land cover. As a possible solution to this restriction, future algorithms may develop spatial change masks using multi-date Landsat observations first and use MODIS to predict the dates at which a change occurred (as the date when the change in pixel brightness occurred). Changes will also not be detected by STARFM when two contradicting changes occur within a coarse-resolution pixel simultaneously and compensate for each other (Gao et al., 2006).

A further assumption made in this analysis is the statement that the MODIS data used in this study represented the "true" vegetation trajectory. MODIS observations are, even more than Landsat, subject to variations in atmospheric conditions and bi-directional reflectance distribution and as a result, these effects introduce uncertainties to variations in the visible and NIR reflectance. Data smoothing techniques such as TimeSat (Jonsson & Eklundh, 2004) may be helpful to address this issue in future research. Further uncertainties are added by spatial and spectral variations between the two sensors.

The results shown in this study largely focussed on coniferous forest types, which are typical for large parts of Western Canada. Further research needs to be done in order to investigate the potential of using STARFM also in other regions of the earth, such as tropical or temperate deciduous forests. Cloud contamination in Landsat or MODIS T_1 scenes has implications for the practical use of the algorithm, as predictions can only be made if at least one completely cloud-free observation is available for the period of interest. While this may be less constraining in temperate climatic zones and at regional scales, the availability of cloud-free observations becomes a major concern over larger areas or when operating at global scales (Ju et al., 2007). Composition of multiple Landsat scenes with observation dates noted for each pixel may help to overcome this issue, as STARFM predictions could be made on composites of both Landsat and MODIS images.

5. Conclusion

- The STARFM algorithm has been successfully used in this study to map seasonal changes in vegetation at a Landsat spatial resolution and 8-day time intervals.
- The algorithm has maintained a high spatial level of detail in the predicted scenes, it seems however, less well suited to predict sudden changes in land cover, such as induced by stand replacing disturbance events.
- The use of MODIS composites can be a useful alternative to daily observations, especially when cloud cover prevents frequent clear sky observations of a given area. Composites may however reduce the quality of STARFM predictions due to changes in pixel brightness resulting from remaining directional or atmospheric impacts in the different MODIS images (for instance the relationship between all observed and predicted Landsat images revealed a slope <1 and intercept >0).

Acknowledgements

Funding for this research was generously provided by the Grizzly Bear Program of the Foothills Research Institute located in Hinton, Alberta, Canada, with additional information available at: http://www.fmf.ab.ca/. Much of the Landsat data used in this study was contributed by the U.S. Geological Survey Landsat Data Continuity

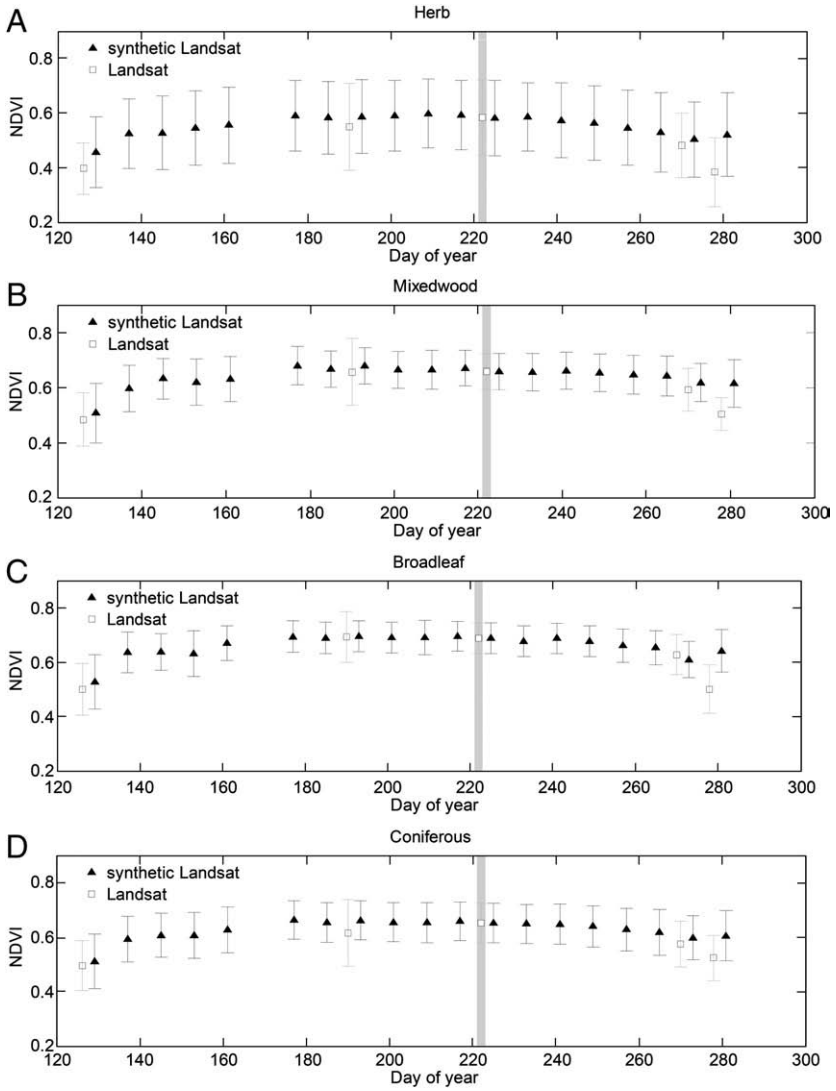

Fig. 8. Eight-day time series of mean NDVI values calculated for the most common land cover types between DOY 120 to 280 (2001). The triangles show the mean NDVI values derived from STARFM synthetic images, the corresponding errorbars represent the standard deviation. The open squares mean NDVI values derived from the actual Landsat observations, the errorbars represent the standard deviation. The grey line at DOY 226 marks the T_1 date which was used for the STARFM predictions. Synthetic NDVI observations fit well into the annual pattern of the vegetation cycle for the different land cover types. Greatest differences in reflectance due to seasonal effects were found for the broadleaf vegetation class ($\Delta NDVI_{max} = 0.21$), while the coniferous land cover type maintained a more homogeneous level of NDVI ($\Delta NDVI_{max} = 0.16$).

Mission Project through participation of Wulder on the Landsat Science Team. The anonymous reviewers are thanked for a thorough review of this manuscript.

References

Acerbi-Junior, F. W., Clevers, J., & Schaepman, M. E. (2006). The assessment of multi-sensor image fusion using wavelet transforms for mapping the Brazilian savanna. *International Journal of Applied Earth Observation and Geoinformation*, *8*, 278–288.

Asrar, G., Fuchs, M., Kanemasu, E. T., & Hatfield, J. L. (1984). Estimating Absorbed Photosynthetic Radiation and Leaf-Area Index From Spectral Reflectance in Wheat. *Agronomy Journal*, *76*, 300–306.

Busetto, L., Meroni, M., & Columbo, R. (2007). Combining medium and coarse spatial resolution satellite data to improve the estimation of sub-pixel NDVI time series. *Remote Sensing of Environment*, *112*, 118–131.

Carper, W. J., Lillesand, T. M., & Kiefer, R. W. (1990). The use of intensity–hue-saturation transformations for merging SPOT panchromatic and multispectral image data. *Photogrammetric Engineering and Remote Sensing*, *56*, 459–467.

Cohen, W. B., & Goward, S. M. (2004). Landsat's role in ecological applications of remote sensing. *Bioscience*, *54*, 535–545.

Coops, N. C., Johnson, M., Wulder, M. A., & White, J. C. (2006). Assessment of QuickBird high spatial resolution imagery to detect red attack damage due to mountain pine beetle infestation. *Remote Sensing of Environment*, *103*, 67–80.

Drake, B. G. (1976). Seasonal changes in reflectance and standing crop biomass in three salt marsh communities. *Plant Physiology*, *58*, 696–699.

Daughtry, C. S. T., Gallo, K. P., & Bauer, M. E. (1983). Spectral Estimates of Solar-Radiation Intercepted by Corn Canopies. *Agronomy Journal*, *75*, 527–531.

Eklundh, L., Harrie, L., & Kuusk, A. (2001). Investigating relationships between Landsat ETM plus sensor data and leaf area index in a boreal conifer forest. *Remote Sensing of Environment*, *78*, 239–251.

Franklin, S. E., & Wulder, M. A. (2002). Remote sensing methods in medium spatial resolution satellite data land cover classification of large areas. *Progress in Physical Geography*, *26*, 173–205.

Gao, F., Masek, J., Schwaller, M., & Hall, H. (2006). On the blending of the Landsat and MODIS surface reflectance: Predicting daily Landsat surface reflectance. *IEEE Transactions on Geosciences and Remote Sensing*, *44*, 2207–2218.

Hall, F., Sellers, P., Strebel, D., Kanemasu, E., Kelly, R., Blad, B., Markham, B., Wang, J., & Huemmrich, F. (1991). Satellite remote sensing of surface energy and mass balance results: Results from FIFE. *Remote Sensing of Environment*, *35*, 187–199.

Hansen, M. C., Roy, D. P., Lindquist, E., Adusei, B., Justice, C. O., & Altstatt, A. (2008). A method for integrating MODIS and Landsat data for systematic monitoring of forest cover and change in the Congo Basin. *Remote Sensing of Environment*, *112*, 2495–2513.

Holben, B. N. (1986). Characteristics of Maximum-Value Composite Images from Temporal Avhrr Data. *International Journal of Remote Sensing*, *7*, 1417–1434.

Irish, J. (2000). Landsat 7 Automatic Cloud Cover Assessment. In S. S. Shen & M. R. Descour (Eds.), *SPIE/AeroSense 2000, Algorithms for Multispectral, Hyperspectral, and Ultraspectral Imagery* (pp. 348–355).

Irish, R. R., Barker, J. L., Goward, S. N., & Arvidson, T. (2006). Characterization of the Landsat-7 ETM+ automated cloud-cover assessment (ACCA) algorithm. *Photogrammetric Engineering and Remote Sensing*, *72*, 1179–1188.

Jonsson, P., & Eklundh, L. (2004). TIMESAT — A program for analyzing time-series of satellite sensor data. *Computers and Geosciences*, *30*, 822–845.

Ju, J. C., & Roy, D. P. (2007). The availability of cloud-free Landsat ETM+ data over the conterminous United States and globally. *Remote Sensing of the Environment*, *112*, 1196—1211.

Justice, C. O., Townshend, J. R. G., Holben, B. N., & Tucker, C. J. (1985). Analysis of the Phenology of Global Vegetation Using Meteorological Satellite Data. *International Journal of Remote Sensing*, *6*, 1271—1318.

Kalvelage, T., & Willems, J. (2005). Supporting users through integrated retrieval, processing, and distribution systems at the Land Processes Distributed Active Archive Center. *Acta Astronautica*, *56*, 681—687.

Leckie, D. (1990). Advances in remote sensing technologies for forest surveys and management. *Canadian Journal of Forest Research*, *21*, 464—483.

Masek, J. G., & Collatz, G. J. (2006). Estimating forest carbon fluxes in a disturbed southeastern landscape: Integration of remote sensing, forest inventory, and biogeochemical modeling. *Journal of Geophysical Research-Biogeosciences*, 111.

Maxwell, S. K., Schmidt, G. L., & Storey, J. C. (2007). A multi-scale approach to filling gaps in Landsat ETM+ SLC-off images. *International Journal of Remote Sensing*, *28*, 5339—5356.

Meidinger, D., & Pojar, J. (1991). *Ecosystems of British Columbia* (pp. 330). Victoria, BC: Province of British Columbia.

Myneni, R. B., & Williams, D. L. (1994). On the Relationship Between Fapar and Ndvi. *Remote Sensing of Environment*, *49*, 200—211.

Pape, A. D., & Franklin, S. E. (2008). MODIS-based change detection for Grizzly Bear habitat mapping in Alberta. *Photogrammetric Engineering and Remote Sensing*, *74*, 973—985.

Patenaude, G., Milne, R., & Dawson, T. P. (2005). Synthesis of remote sensing approaches for forest carbon estimation: Reporting to the Kyoto Protocol. *Environmental Science & Policy*, *8*, 161—178.

Peddle, D., Hall, F., & LeDrew, E. (1999). Spectral mixture analysis and geometric optical reflectance modeling of boreal forest biophysical structure. *Remote Sensing of Environment*, *67*, 288—297.

Prince, S. D. (1991). Satellite remote-sensing of primary production — Comparison of results for Sahelian grasslands 1981–1988. *International Journal of Remote Sensing*, *12*, 1301—1311.

Prince, S. D., & Goward, S. N. (1995). Global primary production: A remote sensing approach. *Journal of Biogeography*, *22*, 815—835.

Ranson, K. J., Kovacs, K., Sun, G., & Kharuk, V. I. (2003). Disturbance recognition in the boreal forest using radar and Landsat-7. *Canadian Journal of Remote Sensing*, *29*, 271—285.

Roy, P., Junchang, J., Lewis, P., Schaaf, C., Gao, F., Hansen, M., & Lindquist, E. (2008). Multi-temporal MODIS–Landsat data fusion for relative radiometric normalization, gap filling, and prediction of Landsat data. *Remote Sensing of Environment*, *112*, 3112—3130.

Sellers, P. J. (1985). Vegetation-canopy spectral reflectance and biophysical processes. In G. Asrar (Ed.), *Theory and applications of optical remote sensing* (pp. 297—335). New York: Wiley.

Sellers, P. J., Randall, D. A., Collatz, G. J., Berry, J. A., Field, C. B., Dazlich, D. A., Zhang, C., Collelo, G. D., & Bounoua, L. (1996). A revised land surface parameterization (Sib2) for atmospheric Gcms.1. model formulation. *Journal of Climate*, *9*, 676—705.

Shettigara, V. K. (1992). A generalized component substitution technique for spatial enhancement of multispectral images using a higher resolution data set. *Photogrammetric Engineering & Remote Sensing*, *58*, 561—567.

Slaymaker, D., Jones, K., Griffin, C., Finn, J., Scott, J., Tear, T., & Davis, F. (1996). Mapping deciduous forests in southern New England using aerial videography and hyperclustered multi-temporal Landsat TM imagery. *Gap analysis: A landscape approach to biodiversity planning* (pp. 87—101). : American Society of Photogrammetry and Remote Sensing.

Townshend, J., & Justice, C. (1995). Spatial variability of images and the monitoring of changes in the Normalized Difference Vegetation Index. *International Journal of Remote Sensing*, *16*, 2187—2195.

Trishchenko, A. P., Luo, Y., & Khlopenkov, K. V. (2006). A method for downscaling MODIS land channels to 250 m spatial resolution using adaptive regression and normalization. In M. Ehlers, & U. Michel (Eds.), *Remote Sensing for Environmental Monitoring, GIS applications, and Geology VI*, *vol. 6366*. (pp.)Ottawa, ON: Canada Center for Remote Sensing.

Tucker, C. (1979). Red and photographic infrared linear combinations for monitoring vegetation. *Remote Sensing of Environment*, *8*, 127—150.

Vermote, E. F., & Kotchenova, S. Y. (2008). *MOD09 (Surface Reflectance) User's Guide, Version 1.1*. Website available at http://modis-sr.ltdri.org

Wolfe, R. E., Nishihama, M., Fleig, A. J., Kuyper, J. A., Roy, D. P., Storey, J. C., & Patt, F. S. (2002). Achieving sub-pixel geolocation accuracy in support of MODIS land science. *Remote Sensing of Environment*, *83*, 31—49.

Wu, J. D., Wang, D., & Bauer, M. E. (2005). Image-based atmospheric correction of QuickBird imagery of Minnesota cropland. *Remote Sensing of Environment*, *99*, 315—325.

Wulder, M. A., Dechka, J. A., Gillis, M. A., Luther, J. E., Hall, R. J., & Beaudoin, A. (2003). Operational mapping of the land cover of the forested area of Canada with Landsat data: EOSD land cover program. *The Forestry Chronicle*, *79*, 1075—1083.

Wulder, M. A., White, J. C., Goward, S. N., Masek, J. G., Irons, J. R., Herold, M., Cohen, W. B., Loveland, T. R., & Woodcock, C. E. (2008). Landsat continuity: Issues and opportunities for land cover monitoring. *Remote Sensing of Environment*, *112*, 955—969a.

Wulder, M. A., White, J. C., Magnussen, S., & McDonald, S. (2007). Validation of a large area land cover product using purpose-acquired airborne video. *Remote Sensing of Environment*, *106*, 480—491.

Yocky, D. A. (1996). Multiresolution wavelet decomposition image merger of Landsat Thematic Mapper and SPOT panchromatic data. *Photogrammetric Engineering & Remote Sensing*, *62*, 1067—1074.